Patterning of Heteroepitaxial Overlayers from Nano to Micron Scales

K. R. Elder,[1,*] G. Rossi,[2] P. Kanerva,[2] F. Sanches,[1] S-C. Ying,[3] E. Granato,[3,4] C. V. Achim,[2] and T. Ala-Nissila[2,3]

[1]*Department of Physics, Oakland University, Rochester, Michigan 48309, USA*

[2]*Department of Applied Physics and COMP Centre of Excellence, Aalto University School of Science, P.O. Box 11000, FI-00076 Aalto, Espoo, Finland*

[3]*Department of Physics, Brown University, P.O. Box 1843, Providence, Rhode Island 02912, USA*

[4]*Laboratório Associado de Sensores e Materiais, Instituto Nacional de Pesquisas Espaciais, 12227-010 São José dos Campos, SP, Brazil*

(Received 22 December 2011; published 29 May 2012)

Thin heteroepitaxial overlayers have been proposed as templates to generate stable, self-organized nanostructures at large length scales, with a variety of important technological applications. However, modeling strain-driven self-organization is a formidable challenge due to different length scales involved. In this Letter, we present a method for predicting the patterning of ultrathin films on micron length scales with atomic resolution. We make quantitative predictions for the type of superstructures (stripes, honeycomb, triangular) and length scale of pattern formation of two metal-metal systems, Cu on Ru(0001) and Cu on Pd(111). Our findings are in excellent agreement with previous experiments and call for future experimental investigations of such systems.

DOI: 10.1103/PhysRevLett.108.226102 PACS numbers: 68.55.−a, 68.35.bd, 68.35.Gy, 81.10.Aj

The understanding of structure-property relations in metal surfaces and the control of pattern formation are nowadays key technological issues. The ordering of the reactants on a patterned surface [1], the nucleation and growth of graphene on metal films [2–6], the self-organization of two-dimensional (2D) vacancy islands at an heterogeneous metal interface [7,8] are all processes driven by a subtle interplay of adhesion and strain energy contributions at the metal surface. In some cases, such as on Au, Ir, and Pt surfaces [9–12], the reduced dimensionality of the surface is the only driving force leading to surface reconstruction. More often, surface patterning arises in heteroepitaxial systems, where the strain is generated at the interface between metals with different bulk lattice constants. This occurs when Cu, Ni, or Co are deposited on the compact surface of Ru [13–15], and similarly in Ni on Rh(111), Co on Pd(111), and Cu on Pd(111) [16–18].

From a modeling point of view, different methodologies can shed light on the different processes involved. First-principle calculations are constantly being refined to obtain reliable quantitative estimates of surface and adhesion energies [19]. Often relying on the former, classical potentials coupled to Monte Carlo and molecular dynamics (MD) simulations allow exploration of surfaces in ground state and metastable configurations and of basic diffusion and relaxation processes [18,20,21] whose time and length scale are not yet approachable by first-principles. More recently, metal surface patterning has been approached by means of phase-field crystal (PFC) methods [22–24], as well. In these methods, the local free energy of the system is expressed as a functional of a local atomic density field. The free energy is relaxed in a dissipative way, leading to the identification of ground-state and metastable configurations. The typical time scales associated with free energy relaxation on a metal surface are orders of magnitude larger than those accessible by MD simulations. Nevertheless, the use of both PFC and MD methods is limited by the need to resolve spatial details on the angstrom scale and cannot be used to explore the large sections of metallic surface routinely probed in experiments.

To overcome the spatial limitation of the standard PFC, in this work we will use an amplitude expansion of the density field [25–29]. This methodology allows the study of 2D films adsorbed on a rigid substrate with spatial dimensions of several hundred nanometers, yet retains atomistic resolution. We study the ground and metastable states of heteroepitaxial ultrathin films, where the film lattice constant is smaller than that of the substrate (tensile mismatch). The model quantitatively reproduces the patterns formed by Cu on Ru(0001) in a range of coverage that extends from 1 to 4 monolayers (ML), in striking agreement with experimental data. The model predicts the appearance of similar patterning at other metal-metal interfaces, as well as calling for further experimental investigations.

In our model, the (111) or (0001) surface of the substrate (an fcc or hcp metal, respectively) is approximated by a rigid pinning dimensionless potential, $V = U/k_BT$. V will be set to $V = V_0[\sum_{j=1}^{3} \exp(i\vec{G}_j^s \cdot \vec{r}) + \text{c.c.}]$ where c.c. is the complex conjugate and $\vec{G}_1^s = -q^s(\sqrt{3}\hat{x}/2 + \hat{y}/2)$, $\vec{G}_2^s = q^s\hat{y}$, and $\vec{G}_3^s = q^s(\sqrt{3}\hat{x}/2 - \hat{y}/2)$ are the three reciprocal lattice vectors needed to reconstruct the potential of the (111) surface of the substrate, where $q_s = 2\pi/a_s$, with a_s the lattice constant of the substrate. If V_0 is positive, the maxima of the potential are placed on a triangular lattice

mimicking the presence of the substrate atoms. The minima (adsorption sites) are ordered on a honeycomb lattice, containing two triangular sublattices. On real compact surfaces, these sublattices correspond to the adsorption with fcc or hcp stacking. In our model, fcc and hcp minima are degenerate. This is a reasonable approximation, since for many metal-metal systems the difference between the adsorption energy on fcc and hcp sites is negligible, of the order of 1 meV per atom. Nevertheless, a difference between the adsorption energy of hcp and fcc sites can be easily introduced in the model, as shown in the Supplemental Material [30].

In a PFC model the atomic ordering of the overlayer is described by the normalized local atomic number density difference, n, which is uniform in a liquid state and periodic in the solid phase; i.e., it mimics the symmetry of a given crystalline state. This periodic variation limits the applicability of the model as the grid spacing must be less than the atomic spacing. To overcome this difficulty, an amplitude expansion was developed by Goldenfeld *et al.* [25–29]. In this formulation the density is expanded around the basis set as the substrate, i.e., $n = \sum \eta_j e^{i\vec{G}_j^s \cdot \vec{r}} + \text{c.c.}$, where η_j is a complex amplitude that varies on length scales much larger than $2\pi/|\vec{G}_j^s|$, the film is such that $\vec{G}_j^s = \alpha \vec{G}_j^f$ and the mismatch between the substrate (lattice constant a^s) and film (a^f) is then $\varepsilon \equiv (a^s - a^f)/a^s = (1 - \alpha)$. We incorporate the external surface potential V into the amplitude expansion formulation through the addition of a Vn term to the PFC free-energy functional. This approach has been used to describe incommensurate-commensurate transitions [31,32], sliding friction [33,34], and the ordering of ultrathin binary films [35].

All lengths are scaled such that the fundamental length scale is $a_f/2\pi$ and the amplitude of the coupling potential V_0 is also written in dimensionless form, whose relevance to experimental systems will be discussed below. The resulting equation of motion for the amplitudes can be written $\partial \eta_j/\partial t \approx -\delta F_\eta/\delta \eta_j^*$ or

$$\frac{\partial \eta_j}{\partial t} \approx -(\Delta B + B^x \mathcal{G}_j^2 + 3v(A^2 - |\eta_j|^2))\eta_j + 2\tau \prod_{i \neq j} \eta_i^* - V_0, \quad (1)$$

where $\mathcal{G}_j = \nabla^2 + 2i\alpha \vec{G}_j^f \cdot \vec{\nabla} + 1 - \alpha^2$, $A^2 \equiv 2\sum |\eta_j|^2$, and F_η is the dimensionless free-energy functional. ΔB and B^x control the liquid-solid transition and the magnitude of the elastic constants, respectively. The model differs from previous expansions in two ways. First, it is an expansion about a strained state (instead of unstrained) leading to a modification of the operator $\mathcal{G}_j$, i.e., the $1 - \alpha^2$ term. Second, it includes the influence of a (0001) surface through the V_0 term. Neither of these effects were included in the amplitude expansions discussed in Refs. [25–29] and are essential for describing the phenomena of interest here. While the amplitudes can be used to reconstruct the atomic density n and thus incorporate atomistic details such as dislocations, it should be noted that this description is missing the subtle coupling of the two length scales (a and the variation of η_j) that leads to Peierls barriers [36] and faceting. A detailed description of the derivation of Eq. (1) is given in the Supplemental Material [30].

When the coupling strength is very high ($V_0/\varepsilon^2 \to \infty$), the adsorbate occupies the commensurate state, namely a triangular lattice either on the fcc or the hcp adsorption sites. At low V_0/ε^2 the overlayer floats above the substrate in an incommensurate state. It is straightforward (see Supplemental Material [30]) to show that, for small mismatches, the difference in free energy between the commensurate and the incommensurate states is approximately $F_\eta^c - F_\eta^i \approx -3V_0\phi + 12B^x\varepsilon^2\phi^2$, where ϕ is the amplitude of the density fluctuations. In comparison, the commensurate state energy is lowered by the first term, i.e., coupling to the substrate, but increased by the second term, i.e., the elastic energy needed to stretch the adsorbed layer. The critical value of the dimensionless coupling V_0^*, at which the incommensurate and commensurate states are equal, is then $V_0^* \approx 4B^x\phi\varepsilon^2$, which provides a reference energy scale that can be used to compare with experiment.

When a completely incommensurate layer is superimposed on the substrate, a honeycomb moiré pattern emerges that has a periodicity that is related to the different length scales of the layer and substrate. This periodicity is given by $L_M = 2\pi/(|\vec{G}_j^f| - |\vec{G}_j^s|) = 2\pi/\varepsilon$. Converting back to actual lengths, $\tilde{L}_M = a_f/\varepsilon$. Naturally, this length will play a role in the patterns that emerge in between completely incommensurate and commensurate states.

For intermediate coupling, interesting superstructures are formed. The film atoms periodically shift from fcc to hcp sites, relieving strain at the domain walls separating the two states. Numerical simulations of the model for various initial conditions and parameters indicate that two specific spatial patterns emerge, which we call striped and honeycomb superstructures. They are shown in Fig. 1, where the pattern periodicities are shown as a function of coupling strength at $\varepsilon = 5.5\%$ [as for Cu/Ru(0001)] for both stripe and honeycomb superstructures. As expected, the periodicity of the honeycomb pattern starts at L_M and then increases as V_0 increases in order to enlarge the commensurate regions. At a specific value of V_0 (V_0^{hs}), the free energy per unit area of the honeycomb superstructure becomes larger than that of the striped superstructure. The periodicity of the striped phase increases with V_0 and diverges at the transition to a commensurate state (V_0^{sc}).

Repeating this procedure for other values of ε leads to the phase diagram shown in Fig. 2. Both the honeycomb to stripe and the stripe to commensurate transition coupling strengths, V_0^{hs} and V_0^{sc}, are roughly quadratic in ε, as might

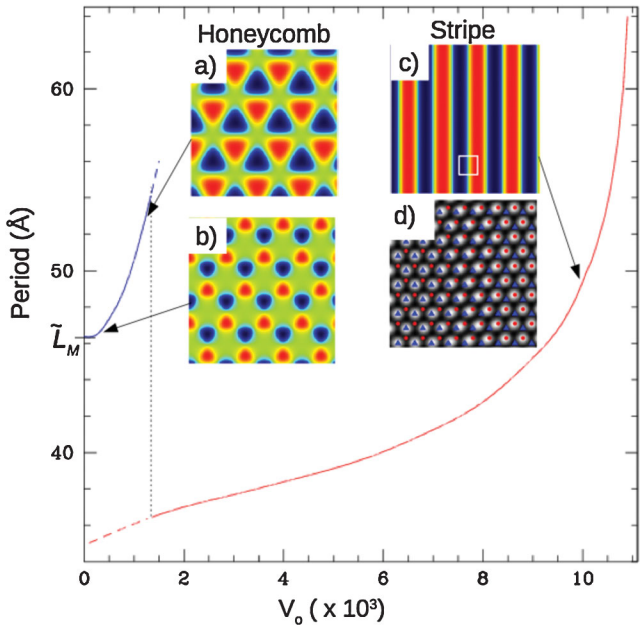

FIG. 1 (color). Equilibrium configurations for Cu/Ru(0001) at a 5.5% mismatch, with honeycomb (a),(b) or striped (c), (d) superstructures. In (a)–(c), fcc domains are blue, hcp domains are red, and domain walls are green. In (d) the gray scale corresponds to a reconstruction of the atomic density for the region enclosed by the white square in (c). Blue triangles (red circles) correspond to fcc (hcp) sites. The graph shows the period of superstructure versus the coupling strength.

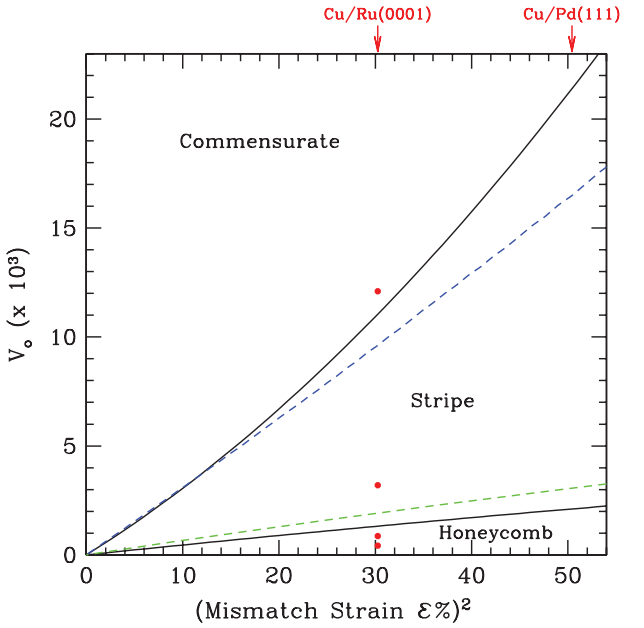

FIG. 2 (color). The solid black lines delineate regions of commensurate, striped, and honeycomb equilibrium states. The dashed blue line corresponds to the 1D sine-Gordon solution for the stripe-commensurate transition. The dashed green line is V_0^*. The data shown in Fig. 1 correspond to wavelength or state selection for Cu/Ru(0001). The relative strain for Cu on Ru(0001) and Pd(111) are also shown in the plot. The red dots from top to bottom correspond to the parameters used in Figs. 3(a)–3(d), respectively.

be expected, since the gain in elastic energy is proportional to ε^2 and the loss in adsorption energy is proportional to V_0. It is possible to estimate the value of $V_0^{\rm sc}$ in the small ε limit by reducing the free energy to a sine-Gordon free-energy functional that has been studied extensively [37]. This can be achieved by assuming $\eta_j = \phi e^{i\theta_j}$, where $\theta_j \approx \theta_j(-\infty) + \frac{2}{3}\vec{G}_j \cdot \vec{\delta}\Phi$ and $\vec{\delta}$ is a unit vector that points from an hcp site to an fcc site, i.e., $\vec{\delta} = \sqrt{3}\hat{x}/2 - \hat{y}/2$. This approximation leads to a free-energy functional in the variable Φ that can be written in sine-Gordon form, i.e., $F_\phi \approx \int d\vec{r}[K/2(\partial\Phi/\partial x - \beta)^2 - V_0\phi/2\cos(\Phi)]$, where K and β are parameters given in the Supplemental Material [30]. Using known results of this free energy, the prediction $V_0^{\rm sc} \approx [9\pi^2 B^x \phi/5]\varepsilon^2$ can be made. It is also interesting to note that this free energy predicts that the selected stripe wavelength diverges as V_0 approaches $V_0^{\rm sc}$ from below.

The equilibrium superstructures we have shown arise from the competition between adhesive and elastic energies, both of which can be varied continuously through the parameters V_0 and ε. In experiments, the elastic moduli and adhesive energy are fixed by the film-substrate properties. Nevertheless, the addition of more layers has the effect of lowering the adhesive-elastic energy ratio. Consequently, we can expect that the patterns that emerge experimentally as a function of layer thickness are consistent with the patterns that emerge theoretically as V_0 is decreased.

In a typical experiment, the film atoms are deposited at low temperatures and then the sample is annealed at higher temperatures. This allows for the formation of long-lived metastable configurations. At coverages larger than a single monolayer, the ordering of the multilayer films most likely initiates from the film-substrate interface. The first monolayer, which is the most influenced by the substrate and thus the closest to the commensurate phase, most likely orders first. In order to mimic this behavior, we started our simulations from a relaxed state with large commensurate patches, with both fcc and hcp stacking, at $V_0 = 0.013$. Then, we decreased V_0 at a rate of 4.333×10^{-9} per unit time and relaxed the system once the target V_0 was reached. As V_0 decreases below $V_0^{\rm sc}$, the fcc and hcp domains begin to break apart to form stripes, typically first ordering through the motion of dislocations that exist at domain edges. Further decreases in V_0 lead to a triangular structure that eventually leads to the honeycomb phase at very small values of V_0. Sample configurations are shown in Fig. 3 and movies of the process can be found in the Supplemental Material [30]. To highlight the nature of the dislocations, a portion of a configuration containing a single dislocation is shown in the inset of Fig. 3(a).

We can now compare these results with theoretical predictions [for Cu/Pd(111)] and experimental results [for Cu/Ru(0001)]. We performed semiempirical calculations

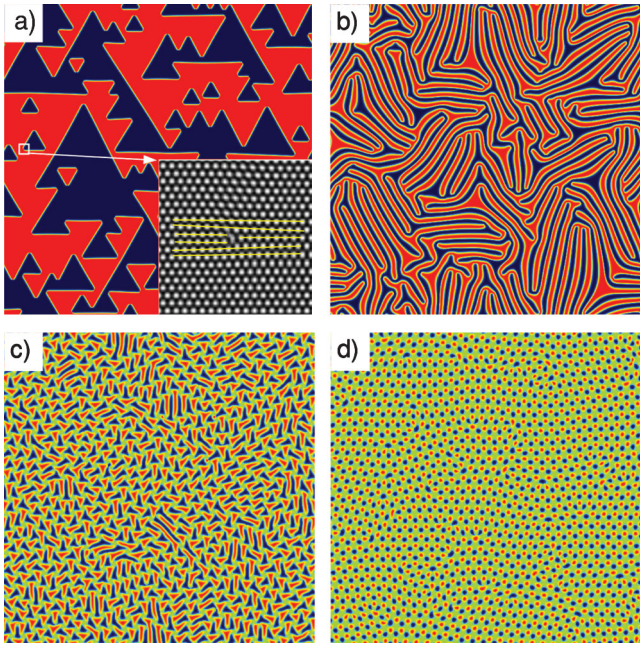

FIG. 3 (color). Spatial patterns obtained at $V_0 = 12.1 \times 10^{-3}$, 3.2×10^{-3}, 0.87×10^{-3}, and 0.43×10^{-3} in (a)–(c), and (d) respectively. The size of each panel is 0.141 μm square. Colors are the same as in Fig. 1 and panels (a)–(d) correspond to the red dots shown in Fig. 2 for Cu/Ru(0001). In the inset, the number density field was reconstructed from the amplitudes for the small region enclosed by the white box. The lines in the inside are a guide to the eye to highlight the point dislocation.

to estimate the value of V_0 for a monolayer of Cu/Pd(111) (7.1% mismatch) as discussed in the Supplemental Material [30]. For a single monolayer, $E_{\rm int}/E_{\rm str} = 4.31$, which would correspond to $V_0 = 4.31V_0^* = 15 \times 10^{-3}$. From Fig. 2 this corresponds to a striped superstructure, which is consistent with experiments and earlier MD studies [18]. The semiempirical calculations also indicate that the ratio $E_{\rm int}/E_{\rm str}$ does indeed decrease as a function of the number of layers, as speculated earlier. While the patterns shown in Fig. 3 are for a mismatch of 5.5%, a similar sequence of patterns was found at 7.1%. It would be interesting to see if these predictions could be verified experimentally as the number of layers is increased.

For Cu/Ru(0001) we could not obtain the ratio $E_{\rm int}/E_{\rm str}$, as no reliable effective interatomic potentials are available. Experiments show that a single monolayer is commensurate with the Ru substrate. In two-monolayer films, striped superstructures have been observed with periodicities of 43 Å [14], 50.7 Å [38], and 55–60 Å [39]. The discrepancies are most likely due to some strain relaxation (thus effectively increasing L_M) from partial Shockley dislocations, as discussed by Figuera *et al.* [39]. Gunther *et al.* [14] also observed triangular type patterns in three-monolayer thick films and honeycomb superstructures in four-monolayer thick films. To compare with these patterns it is important to note that the experimental results only

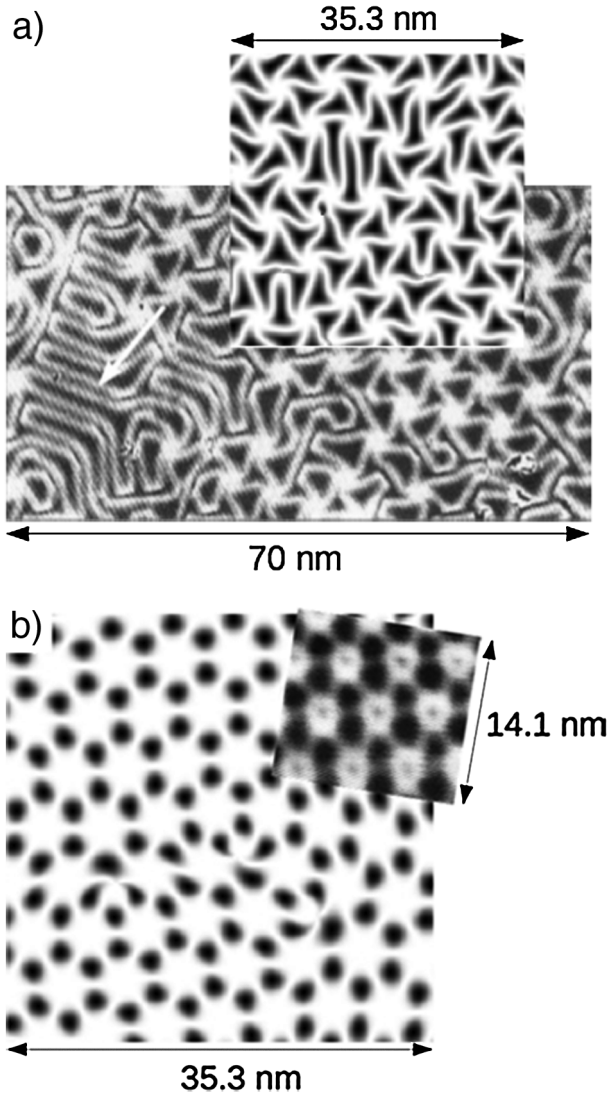

FIG. 4. Comparison between simulated nonequilibrium patterns with experimental results [14] for Cu/Ru(0001). In (a) and (b), the 35.3 nm × 35.3 nm areas correspond to the bottom left quarter of the simulations shown in Figs. 3(c) and 3(d), respectively. In (a) and (b), the 70 nm × 40 nm segment and the 17.2 nm × 14.1 nm segment correspond to three- and four-monolayer results observed by scanning tunneling microscopy by Gunther *et al.* [14].

distinguish between commensurate and incommensurate states (not commensurate fcc and hcp states). We thus expanded some portions of the triangular and honeycomb states shown in Fig. 3, now showing fcc or hcp domains in black and domain walls in white, as shown in Fig. 4. We then overlapped the simulated structures to the experimental pictures of three and four layers in Figs. 4(a) and 4(b), respectively. The length scales of the simulated and experimental systems are in excellent agreement.

In this Letter a method for modeling the structure of stable and metastable heteroepitaxial films on length scales of several hundred nanometers with atomic resolution was

presented. The results of simulations of the model are consistent with existent experimental studies of Cu/Ru(0001) and Cu/Pd(111); at the same time our approach provides insight on the atomic scale. More experimental results are needed in the case of Cu/Pd(111), and the comparison with Cu/Ru(0001) would be significantly enhanced if theoretical predictions could be made for the adhesion-elastic energy ratio as a function of coverage. While the results appear strikingly good, it is important to note that these are 2D calculations that miss some essential physics, such as Shockley partial dislocations [39].

The beauty of using amplitude equations to describe ordering on surface is threefold. First, it predicts patterning on length scales inaccessible to most techniques in the presence of elastic energy and dislocations. Second, since the amplitudes are constant in all of the ordered states, the mesh size needed in simulations is determined only by the length scales of the patterning. Thus it would be straightforward to use adaptive mesh refinement schemes and access scales at least one order of magnitude larger. Third, the method can be extended for substrates of different symmetry by simply expanding around the appropriate reciprocal lattice vectors.

K. R. E. acknowledges support from NSF under Grant No. DMR-0906676. This work has been supported in part by the Academy of Finland through its COMP CoE grant. E. G. was supported by Fundação de Amparo à Pesquisa do Estado de São Paulo—FAPESP (Grant No. 07/08492-9). We also thank CSC—IT Center for Science Ltd. for allocation of computational resources.

*elder@oakland.edu

[1] R. Otero, F. Calleja, V. M. Garcïa-Suärez, J. J. Hinarejos, J. de la Figuera, J. Ferrer, A. L. V. de Parga, and R. Miranda, Surf. Sci. **550**, 65 (2004).
[2] P. Sutter, J. T. Sadowski, and E. Sutter, Phys. Rev. B **80**, 245411 (2009).
[3] X. Li, W. Cai, J. An, S. Kim, J. Nah, D. Yang, R. Piner, A. Velamakanni, I. Jung, and E. Tutuc *et al.*, Science **324**, 1312 (2009).
[4] R. Grantab, V. B. Shenoy, and R. S. Ruoff, Science **330**, 946 (2010).
[5] J. F. Gao, J. Yip, J. J. Zhao, B. I. Yakobson, and F. Ding, J. Am. Chem. Soc. **133**, 5009 (2011).
[6] Z. Sun, S. K. Hämäläinen, J. Sainio, J. Lahtinen, D. Vanmaekelbergh, and P. Liljeroth, Phys. Rev. B **83**, 081415(R) (2011).
[7] K. Pohl, M. C. Bartelt, J. de la Figuera, N. C. Bartelt, J. Hrbek, and R. Q. Hwang, Nature (London) **397**, 238 (1999).
[8] K. Ait-Mansour, A. Buchsbaum, P. Ruffieux, M. Schmid, P. Groning, P. Varga, R. Fasel, and O. Groning, Nano Lett. **8**, 2035 (2008).
[9] C. B. Carter and R. Q. Hwang, Phys. Rev. B **51**, 4730 (1995).
[10] C. Busse and T. Michely, Surf. Sci. **552**, 281 (2004).
[11] T. Michely, M. Hohage, S. Esch, and G. Comsa, Surf. Sci. **349**, L89 (1996).
[12] R. Pushpa and S. Narasimhan, Phys. Rev. B **67**, 205418 (2003).
[13] F. E. Gabaly, W. L. W. Ling, K. F. McCarty, and J. de la Figuera, Science **308**, 1303 (2005).
[14] C. Gunther, J. Vrijmoeth, R. Q. Hwang, and R. J. Behm, Phys. Rev. Lett. **74**, 754 (1995).
[15] S.-F. Ding, S.-R. Deng, H.-S. Lu, Y.-L. Jiang, G.-P. Ru, D. W. Zhang, and X.-P. Qu, J. Appl. Phys. **107**, 103534 (2010).
[16] A. Wander, C. J. Barnes, L. D. Mapledoram, and D. A. King, Surf. Sci. **281**, 42 (1993).
[17] M. Wasniowska, W. Wulfhekel, M. Przybylski, and J. Kirschner, Phys. Rev. B **78**, 035405 (2008).
[18] J. Jalkanen, G. Rossi, O. Trushin, E. Granato, T. Ala-Nissila, and S.-C. Ying, Phys. Rev. B **81**, 041412 (2010).
[19] L. Schimka, J. Harl, A. Stroppa, A. G. Grüneis,, M. Marsman, F. Mittendorfer, and G. Kresse, Nature Mater. **9**, 741 (2010).
[20] T. Marten, O. Hellman, A. V. Ruban, W. Olovsson, C. Kramer, J. P. Godowski, L. Bech, Z. Li, J. Onsgaard, and I. A. Abrikosov, Phys. Rev. B **77**, 125406 (2008).
[21] A. Bergbreiter, H. E. Hoster, S. Sakong, A. Grob, and R. J. Behm, Phys. Chem. Chem. Phys. **9**, 5127 (2007).
[22] K. R. Elder, M. Katakowski, M. Haataja, and M. Grant, Phys. Rev. Lett. **88**, 245701 (2002).
[23] K. R. Elder and M. Grant, Phys. Rev. E **70**, 051605 (2004).
[24] K. R. Elder, N. Provatas, J. Berry, P. Stefanovic, and M. Grant, Phys. Rev. B **75**, 064107 (2007).
[25] N. Goldenfeld, B. P. Athreya, and J. A. Dantzig, Phys. Rev. E **72**, 020601(R) (2005).
[26] B. P. Athreya, N. Goldenfeld, and J. A. Dantzig, Phys. Rev. E **74**, 011601 (2006).
[27] D. H. Yeon, Z.-F. Huang, K. R. Elder, and K. Thornton, Philos. Mag. **90**, 237 (2010).
[28] K. R. Elder, Z.-F. Huang, and N. Provatas, Phys. Rev. E **81**, 011602 (2010).
[29] Z.-F. Huang, K. R. Elder, and N. Provatas, Phys. Rev. E **82**, 021605 (2010).
[30] See Supplemental Material http://link.aps.org/supplemental/10.1103/PhysRevLett.108.226102 for a brief description of the amplitude model, its connection to the sine-Gordon model, some sample movies of the ordering dynamics, and a brief description of the semiempirical calculations.
[31] C. V. Achim, M. Karttunen, K. R. Elder, E. Granato, T. Ala-Nissila, and S. C. Ying, Phys. Rev. E **74**, 021104 (2006).
[32] J. A. P. Ramos, E. Granato, C. V. Achim, S. C. Ying, K. R. Elder, and T. Ala-Nissila, Phys. Rev. E **78**, 031109 (2008).
[33] C. V. Achim, J. A. P. Ramos, M. Karttunen, K. R. Elder, E. Granato, T. Ala-Nissila, and S. C. Ying, Phys. Rev. E **79**, 011606 (2009).
[34] J. A. P. Ramos, E. Granato, S. C. Ying, C. V. Achim, K. R. Elder, and T. Ala-Nissila, Phys. Rev. E **81**, 011121 (2010).
[35] S. Muralidharan and M. Haataja, Phys. Rev. Lett. **105**, 126101 (2010).
[36] R. Peierls, Proc. Phys. Soc. London **52**, 34 (1940).
[37] P. M. Chaikin and T. C. Lubensky, *Principles of Condensed Matter Physics* (Cambridge University Press, Cambridge, England, 1995).
[38] A. K. Schmid, N. C. Bartelt, J. C. Hamilton, C. B. Carter, and R. Q. Hwang, Phys. Rev. Lett. **78**, 3507 (1997).
[39] J. de la Figuera, A. K. Schmid, N. C. Bartelt, K. Pohl, and R. Q. Hwang, Phys. Rev. B **63**, 165431 (2001).